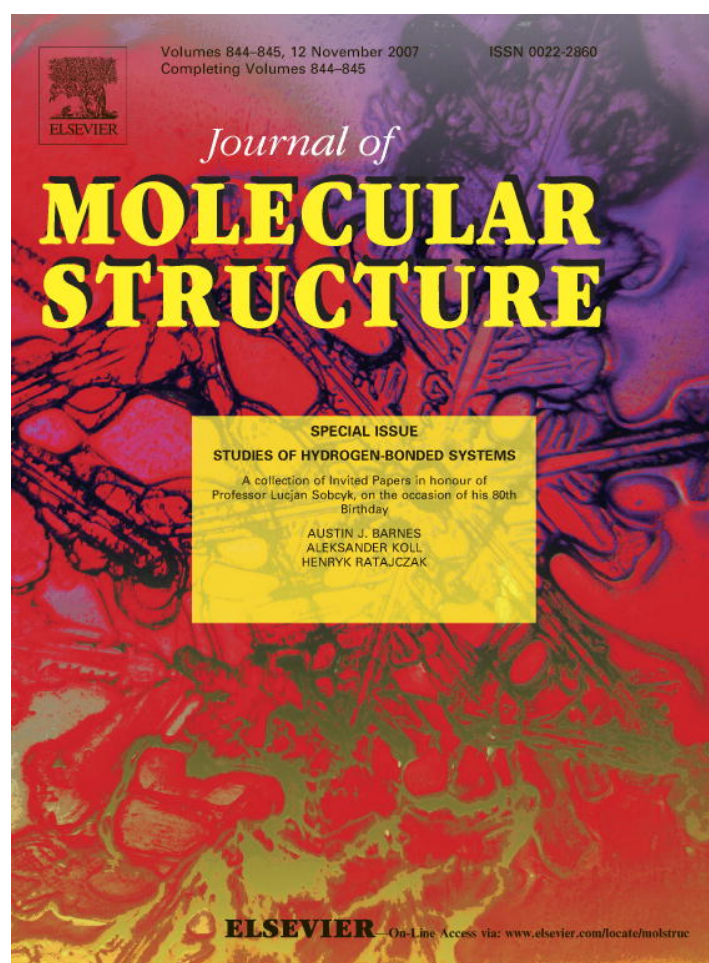


Provided for non-commercial research and education use.
Not for reproduction, distribution or commercial use.



This article was published in an Elsevier journal. The attached copy is furnished to the author for non-commercial research and education use, including for instruction at the author's institution, sharing with colleagues and providing to institution administration.

Other uses, including reproduction and distribution, or selling or licensing copies, or posting to personal, institutional or third party websites are prohibited.

In most cases authors are permitted to post their version of the article (e.g. in Word or Tex form) to their personal website or institutional repository. Authors requiring further information regarding Elsevier's archiving and manuscript policies are encouraged to visit:

<http://www.elsevier.com/copyright>



Proton transfer in the KHCO_3 and benzoic acid crystals: A quantum view

François Fillaux *

LADIR-CNRS, UMR 7075, Université Pierre et Marie Curie, 2 rue Henry Dunant, 94320 Thiais, France

Received 22 March 2007; received in revised form 23 May 2007; accepted 28 May 2007

Available online 23 June 2007

It is a great pleasure to dedicate this paper to Professor Lucjan Sobczyk on the occasion of his eightieth birthday, and to wish him many more happy and productive years of activity in chemistry.

Abstract

A quantum rationale is formulated for proton dynamics in crystals composed of hydrogen bonded centrosymmetric dimers. The purpose is to account for experimental data from various techniques: diffraction, solid-state NMR, quasi-elastic neutron scattering, and vibrational spectroscopy. Spatially coherent distributions, adiabatic separation, nonlocal dynamics, and quantum interferences, are opposed to statistical disorder, semiclassical dynamics, local double-well potentials and stochastic jumps. The tunnelling-level schemes, determined from spectroscopy data, evidence different interconversion mechanisms: adiabatic two-stepwise for KHCO_3 ; coherent phonon-assisted tunnelling for benzoic acid. This latter can be further decomposed into single-step pairwise, single-step single-particle, and single-step two-particles processes. Calculated proton distributions and fluctuation rates at thermal equilibrium are in rather good agreement with measurements.

© 2007 Elsevier B.V. All rights reserved.

Keywords: Hydrogen bonding; Quantum entanglement; Proton transfer; Tunneling; Spectroscopy

1. Introduction

This paper is a very preliminary attempt aiming at the formulation of a quantum framework for proton transfer across $\text{OH} \cdots \text{O}$ hydrogen bonds. There is a general agreement that protons behave as light particles, strongly coupled to heavy atoms, with marked quantum effects, and great sensitivity to isotope substitution. In the condensed matter, long-range effects may arise from large changes of the dipolar moment induced by proton transfer. In order to avoid complications due to such long-range interaction, this paper focuses on crystals composed of centrosymmetric dimers, free of permanent polarization. Such dimers can be found in two configurations, say L and R, related to one

another through the center of symmetry, and in a proportion depending dramatically on the temperature. The interconversion process at issue in this paper should shed some light onto the profound nature of the hydrogen bond, and an in depth understanding of the mechanism is expected to be of importance to many fields across physics, chemistry, or biology [1–5].

The best studied examples are potassium hydrogen carbonate (KHCO_3) [6–22] (Fig. 1), and benzoic acid ($\text{C}_6\text{H}_5\text{OH}$, BA) [23–47] (Fig. 2). Structures and dynamics have been thoroughly investigated, with various techniques and theoretical methods. However, this diversity has led to conflicting interpretations, which can be featured as follows.

On the one hand, vibrational spectroscopy techniques (infrared, Raman, and inelastic neutron scattering-INS) probe dynamics at the rather short time scale of $\sim 10^{-12}$ – 10^{-15} s. Energy-levels evidence the quantum nature of

* Corresponding author.

E-mail address: fillaux@glvt-cnrs.fr

URL: <http://ulyse.glv-t-cnrs.fr/ladir/pagefillaux.htm>

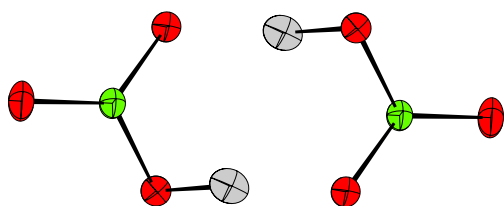


Fig. 1. Schematic view of the centrosymmetric dimers $(\text{HCO}_3^-)_2$ of the KHCO_3 crystal. For the sake of clarity, only one of the proton sites, along the hydrogen bond, is shown.

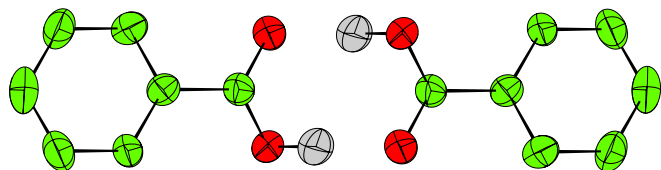


Fig. 2. Schematic view of the centrosymmetric dimers of the benzoic acid. For the sake of clarity, only one of the proton sites, along the hydrogen bond, is shown, and protons of the aromatic rings are omitted.

nuclear dynamics, and double-well potentials can be guessed for proton displacements along the hydrogen bond [9,10,13,18–20,22,37,44]. Quantum dynamics are observed from cryogenic to room temperatures, without any evidence for transition to the classical regime. In principle, the temperature dependence of the interconversion degree, and rate, are directly related to energy levels, but unquestionable assignment schemes are discouragingly difficult to establish.

On the other hand, with solid-state NMR and quasi-elastic neutron scattering (QENS) techniques, one measures kinetics of fluctuations of the probability-density for protons at different sites [23,27,28,32,33,36,39,40,43,45,47]. The time-scale probed by these techniques (longer than $\sim 10^{-12}$ s) is too long to convey direct information on energy levels, and interpretational models are necessary. In the most popular approach, interconversion is supposed to occur through uncorrelated jumps of proton pairs in an asymmetric double-well [27]. In the simplest approximation, the complex evolution of the interconversion rate with the temperature is represented with two dynamical regimes: “incoherent tunnelling” prevailing at low temperatures and semiclassical jumps with Arrhenius behaviour taking the lead at elevated temperatures. However, the question as to whether the two regimes coexist at all temperatures [43,47] or, alternatively, if there is a temperature threshold above which tunnelling is cancelled [36,45] is under debate.

In addition, the space–time-averaged distribution of the nuclear probability-densities can be measured with single-crystal neutron diffraction. The temperature dependent population of proton sites for L and R configurations can be interpreted either in terms of disorder [8,14,30,31], or with spatially-coherent nonlocal distributions [20,22].

The purpose of the present paper is to formulate an interpretational framework consistent with all observations

available, on any time scale longer than $\sim 10^{-15}$ s, at any temperature up to ≈ 300 K. The main points at issue are as follows. First, is it possible to distinguish, with neutron diffraction, disorder from nonlocal distributions? Second, is the adiabatic separation of proton dynamics compatible with strong coupling to heavy atoms? Third, which representation, local or nonlocal, is appropriate for proton dynamics? Fourth, what is the potential function for proton transfer? Fifth, is there any convincing evidence for quantum-to-classical transitions at elevated temperatures? Thorough examination of these questions, throughout the whole ranges of temperatures and time-scales under consideration, will emphasize that interconversion arises from the quantum superposition of macroscopic tunnelling states, on the scale of Avogadro’s constant.

2. Neutron diffraction

Single-crystal neutron-diffraction measurements reveal that at low temperatures protons occupy sites corresponding to a unique configuration for dimers, say L. As the temperature is increased, secondary R sites, at ≈ 0.6 Å along the hydrogen bond, are progressively populated and fractional occupation numbers at thermal equilibrium are ρ_R and ρ_L .

If protons are thought of as classical particles, located at one site or another, fractional occupation numbers should be logically interpreted as a random distribution, usually referred to as “disorder” [8,14,30,31]. However, this interpretation is not appropriate because probability densities, determined from Bragg peaks, should have the spatial periodicity of the crystal lattice. Otherwise, any random distribution of occupied and empty sites automatically destroys long-range correlations, and so a significant amount of coherent scattering should collapse into off-Bragg peaks diffuse scattering [48]. Then, the occupation numbers estimated from Bragg-peak intensities, based on the tabulated nuclear scattering lengths, should lead to $\rho_R + \rho_L < 1$. Contrariwise, neutron diffraction gives $\rho_R + \rho_L \approx 1$ within experimental precision for both KHCO_3 [20,22] and benzoic acid crystals [30,31], throughout the studied temperature ranges. There is no evidence for any significant loss of the spatial coherence for protons. Each proton is therefore simultaneously at L and R sites and the transfer degree is $\rho = \rho_R = 1 - \rho_L$.

Furthermore, the crystal structures are represented with $\text{KH}_\rho\text{H}_{1-\rho}\text{CO}_3$ or $\text{C}_6\text{H}_5\text{COOH}_\rho\text{H}_{1-\rho}$ entities, duplicated according to the lattice symmetry. Each entity is everywhere and each dimer is a superposition of all indistinguishable entities. Such nonlocal entities are conceivable exclusively within the framework of quantum mechanics and this quantum coherence is obviously conceptually different from disorder.

Temperature effects on the CO-bond lengths, presented in the subsections below, should be therefore representative of the crystal state as a whole, rather than of a statistical mixture at thermal equilibrium of L and R dimers.

2.1. KHCO_3

Up to room temperature, the crystal symmetry is $P2_1/a$ with four indistinguishable KHCO_3 entities in the unit cell [7,20,22]. Planar centrosymmetric dimer entities $(\text{HCO}_3^-)_2$ (Fig. 1), linked by moderately strong $\text{OH} \cdots \text{O}$ hydrogen bonds, with length $R_{\text{O} \cdots \text{O}} \approx 2.6 \text{ \AA}$, are separated by potassium atoms. Below $\approx 150 \text{ K}$, only configuration L is observed. Between 150 and 300 K, R sites at $\approx 0.6 \text{ \AA}$ from the L ones along the hydrogen bond, are progressively populated, up to a proton transfer (or interconversion) degree $\rho = 0.18$. At $T_c = 318 \text{ K}$, there is a phase transition [12,14,15], but this is beyond the scope of the present paper.

Temperature effects on the single-like (“C–O”) and double-like (“C=O”) bond-lengths are consistent with a linear dependence on ρ (Fig. 3) as:

$$\begin{aligned} R_{\text{C-O}^-}(\rho) &\approx (0.5 - \rho)R_s + (0.5 + \rho)R_{\text{CO}}, \\ R_{\text{C=O}^+}(\rho) &\approx (0.5 - \rho)R_d + (0.5 + \rho)R_{\text{CO}}. \end{aligned} \quad (1)$$

Extrapolation gives: $R_{\text{CO}} \approx 1.30 \text{ \AA}$ ($\rho = 0.5$), for hypothetical C_{2v} carbonate groups in C_{2h} dimers; $R_s \approx 1.39 \text{ \AA}$, and $R_d \approx 1.22 \text{ \AA}$, for single and double bonds of ideal C_s carbonates. Since there is no evidence for a statistical distribution of R_s and R_d bonds [22], Eq. (1) can be rewritten as a continuous variation of the extended electronic state of the crystal, say $|\mathcal{E}(\rho)\rangle$, as:

$$|\mathcal{E}(\rho)\rangle \approx (0.5 - \rho)^{1/2}|C_s\rangle + (0.5 + \rho)^{1/2}|C_{2v}\rangle. \quad (2)$$

The $|C_s\rangle$ state should correspond to hypothetical unbound C_s entities, HCO_3^- , and the $|C_{2v}\rangle$ state to C_{2h} dimers with protons equally distributed among the four (L,R) sites. The energy difference between R and L, $E_R - E_L = E_{C_{2v}} - E_{C_s}$, should be largely temperature independent, and the energy of the hybridized state should depend linearly on ρ as

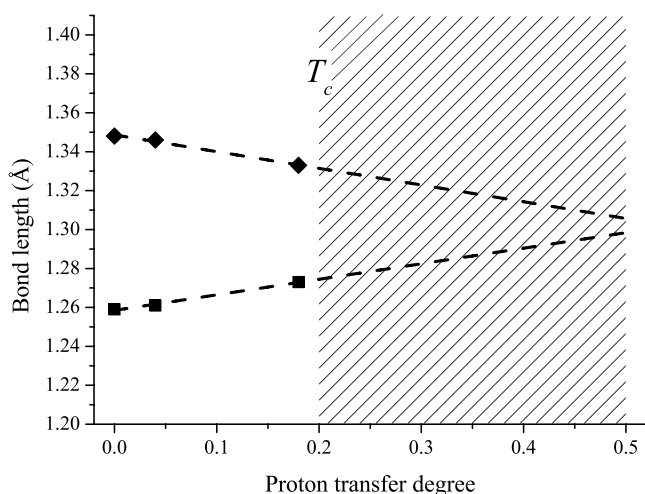


Fig. 3. Correlation of the single-like (■) and double-like (◆) CO bond lengths in the KHCO_3 crystal with the proton transfer degree, after Refs. [20,22]. The hatched area above T_c is unstable. The dash straight lines are the best least-square fits to the experimental points.

$$E(\rho) = (E_{C_{2v}} + E_{C_s})/2 + \rho(E_{C_{2v}} - E_{C_s}), \quad (3)$$

2.2. Benzoic acid

The benzoic acid crystal is also monoclinic $P2_1/c$, with four indistinguishable $\text{C}_6\text{H}_5\text{COOH}$ entities per unit cell. Centrosymmetric dimers (Fig. 2) are linked by hydrogen bonds, with an average $R_{\text{O} \cdots \text{O}}$ of 2.615 Å, between 20 and 175 K [30,31]. There is no phase transition below room temperature. Proton transfer occurs at much lower temperature and ρ ranges from ≈ 0.13 at 20 K to ≈ 0.38 at 175 K.

The evolution of the CO bond lengths with ρ (Fig. 4) shows the same trend as for KHCO_3 , although crystallographic data are less accurate. We extrapolate $R_{\text{CO}} \approx 1.265 \text{ \AA}$, $R_s \approx 1.345 \text{ \AA}$ and $R_d \approx 1.185 \text{ \AA}$. These shorter bonds, compared to KHCO_3 , are representative of the different hybridization states for the two systems. Even if there is no objection to supposing a linear combination of extended electronic states analogous to Eq. (2), more accurate data should be necessary to corroborate this view.

3. Adiabatic separation

Within the framework of the Born–Oppenheimer approximation, the vibrational Hamiltonian for the crystals under consideration can be partitioned as

$$\mathcal{H}_v = \mathcal{H}_H + \mathcal{H}_{\text{at}} + \mathcal{C}_{\text{Hat}}, \quad (4)$$

where \mathcal{H}_H and \mathcal{H}_{at} represent the sublattices of protons (H^+) and heavy atoms, respectively, while \mathcal{C}_{Hat} couples the subsystems. For $\text{OH} \cdots \text{O}$ hydrogen bonds, coupling terms between OH and $\text{O} \cdots \text{O}$ degrees of freedom are rather large [1,49], and beyond the framework of the perturbation theory. This is a major difficulty to modelling dynamics and, because there is no simple solution, two different

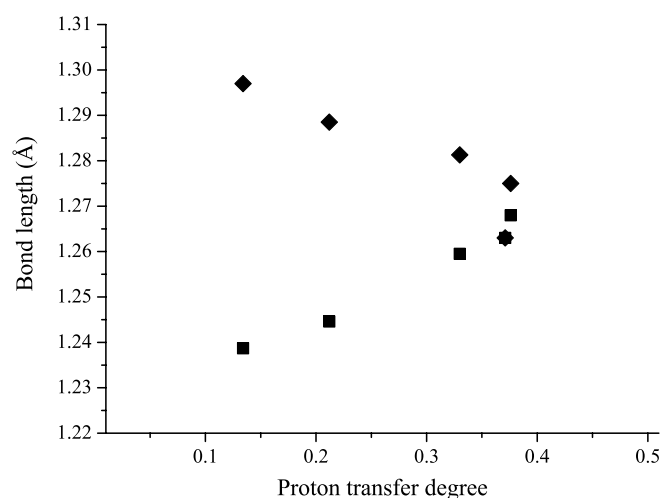


Fig. 4. Correlation of the single-like (■) and double-like (◆) CO bond lengths in the benzoic acid crystal with the proton transfer degree, after Refs. [30,31].

approaches, either semiclassical or quantum, are commonly envisaged.

In the semiclassical view, protons are thought of as dimensionless particles, with definite positions and momentums, moving across a potential energy hypersurface [41,42,50–52]. Complex trajectories, strongly coupled to heavy atoms, lead to mass renormalization, and to incoherent phonon-assisted tunnelling. This approach is quite natural when Born–Oppenheimer surfaces are calculated with quantum chemistry methods, but it may lead to underestimate quantum effects for protons.

Alternatively, if the classical concept of “trajectory” totally alien to quantum mechanics is abandoned, adiabatic separation of the two subsystems \mathcal{H}_H and \mathcal{H}_{at} may lead to tractable models [1,22,44,52–54]. Then, light protons in a definite eigen state should remain in the same state in the course of time, while heavy atoms oscillate slowly, in an adiabatic potential depending on the proton state, through the coupling terms. This separation is relevant for the crystals under consideration because adiabatic potentials do not intersect.

In fact, the separation is rigorously exact in the ground state, since protons should remain in this state for ever, if there is no external perturbation. Furthermore, for asymmetric double-wells, with wave functions largely localized in each well, the separation should also hold for the lower state of the upper minimum. Then, protons should behave as bare quantum particles, and long-live tunnelling states should interfere. Moreover, the adiabatic separation unveils the fermion nature of protons, which leads to quantum correlations that would not occur otherwise [22].

Whether the adiabatic separation is relevant, or not, is not a purely theoretical matter. For KHCO_3 , the separation is very well established, up to room temperature, with neutron scattering experiments [13,19,20,22,55]. For benzoic acid, the interpretation of the INS spectra is more complex [35], and the best evidence is provided by the νOH mode in Raman (Fig. 5) [44]. In contrast to the prevailing opinion that these bands should be broadened by a handful of mechanisms, including non-adiabatic coupling with low frequency $\text{O}\cdots\text{O}$ modes [56,57], the observed bandwidths are actually limited by the resolution function of the spectrometer (a few cm^{-1}), and therefore difficult to estimate. Nevertheless, it transpires that broadening mechanisms, including breaking of the adiabatic separation, are beyond observations and νOH states are essentially stationary. The large frequency shift upon deuteration is a further support to the adiabatic separation.

Let us recall that Raman and infrared spectroscopy probe coherent dynamics at the Brillouin-zone center (BZC, for wave vector $\mathbf{k} = 0$), corresponding to in-phase oscillations of the unit cells throughout the crystal. The discreteness of these extended states is a direct evidence for the quantum regime. By contrast, classical disorder should cancel the $\mathbf{k} = 0$ condition, and the symmetry related selection rules, as well. Clearly, this is not observed for the crys-

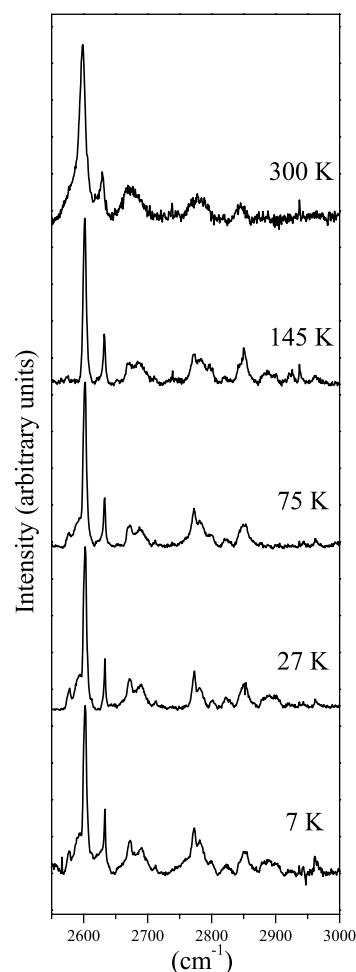


Fig. 5. Raman spectral profiles for a crystal powder of the ring-deuterated benzoic acid at various temperatures.

tals under consideration [6,37,44] (see Fig. 5). Vibrational spectroscopy emphasizes the spatial coherence of the dynamics, on a very short time-scale, complementary to the time-averaged coherence evidenced with neutron diffraction. These experimental facts are quite at variance with the conclusion by Horsewill and coworkers [43,47] that solid-state NMR provides conclusive evidences for a quantum to classical transition, and with the proposal by Latanowicz et al. [36,40,45] of a temperature threshold above which tunnelling should not survive. These conclusions are clearly model dependent. Furthermore, it is argued in the next section that the classical regime is forbidden for the crystals in question.

4. Nonlocal dynamics

In a perfect crystal, atoms are not individual particles possessing properties on their own right. They are entangled. The periodicity and indistinguishability of lattice sites lead to extended states in three dimensions and nonlocal observables (for example phonons). There is no transition to the classical regime, as long as the crystal is stable, and disorder-free.

Because KHCO_3 and benzoic acid crystals have similar symmetries, with two indistinguishable centrosymmetric dimers per unit cell, we can elaborate a theoretical framework for proton dynamics appropriate to both systems. For the sake of clarity, this section is focussed on the ground state ($T = 0$).

4.1. Proton dimers

Consider a monoclinic crystal composed of very large numbers N_a, N_b, N_c ($\mathcal{N} = N_a N_b N_c$) of unit cells labelled j, k, l , along crystal axes (a), (b), (c), respectively. The two dimer entities per unit cell are indexed as j, k, l and j', k', l' , respectively, with $j = j'$, for KHCO_3 , or j, k, l and j, k, l' , with $l = l'$, for benzoic acid. The ground state of a proton dimer is modelled with centrosymmetric collinear harmonic oscillators in three dimensions, along coordinates α_{1jkl} and α_{2jkl} ($\alpha = x, y, z$), each with mass $m = 1$ amu. Then, normal coordinates and conjugated momenta, imposed by the crystal symmetry, irrespective of proton–proton interaction,

$$\begin{aligned} \alpha_s &= \frac{1}{\sqrt{2}} (\alpha_{1jkl} - \alpha_{2jkl}), & P_{sz} &= \frac{1}{\sqrt{2}} (P_{1jklz} - P_{2jklz}), \\ \alpha_a &= \frac{1}{\sqrt{2}} (\alpha_{1jkl} + \alpha_{2jkl}), & P_{az} &= \frac{1}{\sqrt{2}} (P_{1jklz} + P_{2jklz}), \end{aligned} \quad (5)$$

lead to uncoupled harmonic oscillators at frequencies $\hbar\omega_{sz}$ and $\hbar\omega_{az}$, respectively, each with $m = 1$ amu. The Gaussian wave functions, $\Psi_{0jkl}^a(\alpha_a)$, $\Psi_{0jkl}^s(\alpha_s - \sqrt{2}\alpha_0)$, cannot be factored into wave functions for individual particles and there is no local information available for these entangled oscillators. Consequently, the state must be antisymmetrized with respect to permutation of these indistinguishable fermions. For this purpose, the spatial wave function can be rewritten as a linear combination of those for permuted oscillators,

$$\begin{aligned} \Theta_{0jkl\pm} &= \frac{1}{\sqrt{2}} \prod_{\alpha} \Psi_{0jkl}^a(\alpha_a) \\ &\quad \left[\Psi_{0jkl}^s(\alpha_s - \sqrt{2}\alpha_0) \pm \Psi_{0jkl}^s(\alpha_s + \sqrt{2}\alpha_0) \right], \end{aligned} \quad (7)$$

and antisymmetrized state vectors with spin symmetry are:

$$\begin{aligned} |0jkl+\rangle &= |\Theta_{0jkl+}\rangle \otimes \frac{1}{\sqrt{2}} [|\uparrow_1\downarrow_2\rangle - |\downarrow_1\uparrow_2\rangle], \\ |0jkl-\rangle &= |\Theta_{0jkl-}\rangle \otimes \frac{1}{\sqrt{3}} [|\uparrow_1\uparrow_2\rangle + |\downarrow_1\downarrow_2\rangle + \frac{1}{\sqrt{2}} (|\uparrow_1\downarrow_2\rangle + |\downarrow_1\uparrow_2\rangle)]. \end{aligned} \quad (7)$$

The oscillators are now entangled in position, momentum, and spin. In contrast to magnetic systems [58], there is no level splitting, and the symmetry-related entanglement is energy-free. Furthermore, contrariwise to Keen and Lovesey [59], or Sugimoto et al. [60], it is argued, as an experimental fact, that there is no significant overlap of the probability densities for protons at different sites [61]. Protons are not itinerant particles.

Normal coordinates Eq. (5) define nonlocal pseudoprotons ($m = 1$ amu), say \mathcal{P}_{sjkl} and \mathcal{P}_{ajkl} , with an internal degree of freedom corresponding to symmetric or antisymmetric displacements of two “half-protons”, respectively. Each site is a superposition of two such half-protons. Obviously, pseudoprotons are totally alien to the intuitive conception of particles, based on classical mechanics. However, interference fringes, observed with neutron scattering techniques [19,20,22], show that pseudoprotons are observables, whereas local particles are not. Below, it will appear clearly that the concept of pseudoproton is a cornerstone of the interconversion mechanism.

4.2. Macroscopically entangled states

The wave functions of the proton sublattice can be obtained via extension of $\Theta_{0jkl\pm}$, over all indistinguishable sites of the crystal. Consider the trial wave:

$$\Theta_{0\pm}(\mathbf{k}) = \frac{1}{\sqrt{\mathcal{N}}} \sum_{l=1}^{N_c} \sum_{k=1}^{N_b} \sum_{j=1}^{N_a} \Theta_{0jkl\pm} \exp(i\mathbf{k} \cdot \mathbf{L}), \quad (8)$$

where $\mathbf{L} = j\mathbf{a}/2 + k\mathbf{b} + l\mathbf{c}$ and $N'_a = 2N_a, N'_c = N_c$, for KHCO_3 , or $\mathbf{L} = j\mathbf{a} + k\mathbf{b} + l\mathbf{c}/2$ and $N'_a = N_a, N'_c = 2N_c$, for benzoic acid, with the unit cell vectors $\mathbf{a}, \mathbf{b}, \mathbf{c}$. These waves must be antisymmetrical with respect to permutations of j, k, l , and, consequently, $\mathbf{k} \cdot \mathbf{L} \equiv 0$ modulo 2π . There is no phonon (no elastic distortion), and this “super-rigidity” [22] is independent of proton–proton coupling terms. State vectors in three dimensions can be then written as:

$$|0\tau\rangle = |\Theta_{0\tau}(0)\rangle \otimes |\tau\rangle; \quad (9)$$

with $\tau = “+”$ or “ $-$ ” for the singlet-like and triplet-like symmetry, respectively. Each state represents a pseudoproton, \mathcal{P}_a or \mathcal{P}_s , with definite spin-symmetry and occupation numbers of $(4\mathcal{N})^{-1}$ per site. There is no local information available for these macroscopically entangled states. In addition, they are intrinsically decoherence-free. Irradiation by photons, neutrons, etc, may single out some excited pseudoprotons, but as long as Eqs. (5) and (8) remain valid, entanglement in position and momentum is preserved. Only the spin-symmetry and super-rigidity, intrinsic to degenerate states, can be destroyed, but these properties are recovered automatically, after decay to the ground state, presumably on the time-scale of proton dynamics. This mechanism allows the sublattice to be at thermal equilibrium with the surroundings, despite the lack of internal dynamics.

Macroscopic entanglement has been evidenced for KHCO_3 , from 15 to 300 K, with neutron diffraction [20,22]. Thanks to the spin-symmetry, the coherent scattering cross-section for the sublattice of protons is dramatically increased to $\sigma_H \approx 82.0$ barns, compared to the coherent cross-section $\sigma_{\text{CH}} \approx 1.8$ barns for regular Bragg diffraction. The diffraction pattern of the sublattice can be thus observed with remarkable contrast. Thanks to

super-rigidity, the intensity is not attenuated by the Debye–Waller factor at large momentum transfer values and it is little affected by temperature, up to 300 K. The diffraction pattern provides clear evidences that there is no transition to the classical regime and the adiabatic separation is validated over the full temperature range.

For benzoic acid, there is no similar experimental data available, but there is no objection to suppose the same quantum behaviour.

5. Potential surface for proton dynamics

Intra-dimer interactions for protons separated by more than 2 Å are too weak to support the rigid-pair model [27]. On the other hand, uncorrelated transfer of local protons [37] should lead to nonphysical entities, either totally de-protonated, or bi-protonated, in conflict with the symmetry related selection rules observed in the infrared and with Raman [6,37,44]. Clearly, only the quantum concept of pseudoproton is relevant for centrosymmetric dynamics, irrespective of the strength of proton–proton interactions.

Nonlocal double minimum potentials for pseudoprotons, $V(x_a)$ and $V(x_s)$, respectively, were determined from experiments (see Table 1, where energy levels are labelled according to their increasing energy) [9,22,37,44]. The potential asymmetry accounts for the transfer of a pseudoproton without internal excitation, from one well to the other. It should be identical for \mathcal{P}_a and \mathcal{P}_s . On the other hand, excitation of the internal degrees of freedom, ν_a or ν_s , leads to different energy levels in the infrared and Raman, and to slightly different potential barriers. However, the thermal population of these excited states is negligible and such differences can be ignored.

For KHCO_3 , the $|0\rangle \leftrightarrow |1\rangle$ transition was observed with INS [13,17], without visible splitting. The half-width at half-maximum of $\approx 5 \text{ cm}^{-1}$, representative of the density-of-states convoluted with the resolution function, confirms that tunnelling states are virtually dispersion-free. Transitions to upper states were determined from infrared and Raman [10], and the distance between the minima, known from diffraction, determines the effective mass of $\approx 1 \text{ amu}$, in accordance with the adiabatic separation. This potential accounts for a number of observations greater than the number of adjustable parameters [22] and the shape is largely model independent. The ground-state splitting ($h\nu_{01} = 216 \text{ cm}^{-1}$) is dominated by the potential asymmetry, compared to the tunnel splitting for the symmetrized potential: $h\nu_{0t} = 17 \text{ cm}^{-1}$.

Potential functions for the benzoic acid crystal are very similar (see Table 1) [37,44]. For the ring deuterated derivative, the ground state splitting was confirmed with INS, at $h\nu_{01} = 172 \text{ cm}^{-1}$. The transition shows no visible splitting and negligible dispersion. The tunnelling frequency for the symmetrized potential is $h\nu_{0t} = 6 \text{ cm}^{-1}$. The assignment at 172 cm^{-1} was questioned on the basis of DFT calculations [38], but it can be argued that such calculations, based on the harmonic approximation, for a model structure stabilized under an arbitrary pressure, are not appropriate for the determination of double-wells.

For both systems, the barrier heights are largely model and temperature independent. A lower bound is imposed by the νOH transitions observed at $\approx 3000 \text{ cm}^{-1}$, to which should be added a zero-point energy of $\approx 1500 \text{ cm}^{-1}$. Consequently, pseudoproton transfer should occur exclusively via tunnelling, at any temperature. By contrast, potential barriers as low as 460 cm^{-1} [27], or $\approx 330 \text{ cm}^{-1}$ [16,40], are positively excluded, and so are semiclassical proton jumps. The effective mass of $\approx 1 \text{ amu}$ is also model independent, for it is imposed by the known distances between minima. There is no evidence for any significant mass renormalization, suggesting a breaking of the adiabatic separation. Finally, according to Eq. (3), $E_R - E_L = E_{C2v} - E_{Cs} = 2 \times h\nu_{01}$ is primarily due to the electronic structure of the COO groups.

6. Quantum interferences

For the states $|0\rangle$ and $|1\rangle$, the non-antisymmetrized wave functions in one dimension, say x for x_a or x_s , are largely localized in each well. They can be written as [37]:

$$\begin{aligned}\Psi_{0jkl} &= \cos \phi \psi_0(x - x_m) + \sin \phi \psi_0(x + x_m); \\ \Psi_{1jkl} &= -\sin \phi \psi_0(x - x_m) + \cos \phi \psi_0(x + x_m);\end{aligned}\quad (10)$$

where $\psi_0(x - x_m)$ and $\psi_0(x + x_m)$ are harmonic eigen functions for the second-order expansion of the potential around the minima at $\pm x_m$; $\tan 2\phi = \nu_{0t}/(\nu_{01} - \nu_{0t})$ gives: $\cos \phi \approx 1$ and $\sin \phi = \varepsilon \approx 5 \times 10^{-2}$ for KHCO_3 , or $\approx 1.8 \times 10^{-2}$ for benzoic acid. At thermal equilibrium, the superposition of tunnelling states leads to harmonic oscillations of the probability density at the beating frequency: $\nu_{0b} = 8\varepsilon\nu_{01} \approx 4\nu_{0t}$ [37,62].

For dimers, the potential surface

$$\mathcal{V}(x_a, x_s) = V(x_a) + V(x'_s), \quad (11)$$

with $x'_s = x_s \pm \sqrt{2}x_0$, leads to energy levels and non-symmetrized wave functions sketched in Fig. 6 (left hand side). In

Table 1

I: Potential function, distance between the minima, barrier height (H), and energy levels, for KHCO_3 [10,13] and ring deuterated Benzoic acid (BA- d_5h) [37,44]

		$V(x) (\text{cm}^{-1})$	$\Delta x (\text{Å})$	$H_B (\text{cm}^{-1})$	$h\nu_{01} (\text{cm}^{-1})$	$h\nu_{02} (\text{cm}^{-1})$	$h\nu_{03} (\text{cm}^{-1})$
KHCO_3	Raman	$374x + 0.4389 \times 10^6 x^6 + 5516 \exp(-30.8x^2)$	0.60	4850	216*	2475	2820
BA- d_5h	Infrared	$265x + 0.2860 \times 10^6 x^2 + 171480 \exp(-2.17x^2)$	0.70	5005	172*	2570	2840
BA- d_5h	Raman	$270x + 0.2829 \times 10^6 x^2 + 171120 \exp(-2.15x^2)$	0.69	5006	171	2602	2853

* Observed with INS.

the ground state, the two pseudoprotons are in configuration L. In the intermediate state at $h\nu_{01}$, either \mathcal{P}_{ajkl} or \mathcal{P}_{sjkl} , is transferred and there is a half proton at each site. At $2h\nu_{01}$ the two pseudoprotons are transferred. When \mathcal{P}_{ajkl} and \mathcal{P}_{sjkl} are in the same state, the symmetrization postulate leads to antisymmetrized states with spin-symmetry analogous to Eq. (9), which can be written as $|00\tau\rangle$ and $|11\tau\rangle$, respectively. Alternatively, when \mathcal{P}_{ajkl} and \mathcal{P}_{sjkl} are in different configurations, the spin-symmetry is destroyed and plane waves Eq. (8) lead to state vectors $|10, \mathbf{k}_{10}\rangle$ and $|01, \mathbf{k}_{01}\rangle$. Then, superposition of these degenerate states, with the matching condition $\mathbf{k}_{10} = -\mathbf{k}_{01} = \mathbf{k}_1$, leads to energy-free re-entanglement as

$$|10, \mathbf{k}_1\rangle + |01, -\mathbf{k}_1\rangle \leftrightarrow 2^{-1/2} \sum_{\tau} [|00\tau\rangle + |11\tau\rangle]. \quad (12)$$

Consequently, the intermediate state is not stationary but the matching condition for \mathbf{k} may slowdown the re-entanglement process.

6.1. KHCO_3

Owing to the adiabatic separation, energy exchange with the surroundings occurs exclusively via photons, at $\mathbf{k} = 0$.

Then, the intermediate state undergoes fast re-entanglement Eq. (12). The transitory nature of this state is corroborated by the proton transfer degree measured as a function of the temperature (Fig. 7) [22]. If the intermediate state is ignored, $|00\tau\rangle$ and $|11\tau\rangle$ at thermal equilibrium gives

$$\rho(T) = 2p_{01}^2(T)[1 + p_{01}^2(T)]^{-1}, \quad (13)$$

with $p_{01}(T) = \exp(-h\nu_{01}/kT)$. This equation is in reasonably good agreement with measurements (solid line in Fig. 7). By contrast, the transfer degree for the three levels at thermal equilibrium,

$$\rho(T) = [p_{01}(T) + 2p_{01}^2(T)][1 + p_{01}(T) + p_{01}(T)^2]^{-1}, \quad (14)$$

is clearly at variance (dash line in Fig. 7). It is thus confirmed that whereas non-stationary intermediate states $|10, \mathbf{k}_{10}\rangle$ and $|01, \mathbf{k}_{01}\rangle$ can be observed with INS, via energy and momentum transfer, their time-averaged thermal population is negligible, in accordance with Eq. (12). Quite remarkably, vibrational spectroscopy and neutron diffraction converge to virtually the same energy difference of $2 \times h\nu_{01} = 432 \text{ cm}^{-1}$, for R and L configurations.

The interconversion rate can be rationalized as a two-stepwise mechanism. Firstly, either \mathcal{P}_a or \mathcal{P}_s is transferred at $\mathbf{k} = 0$ with probability $\exp(-h\nu_{01}/kT)$. Second, this tran-

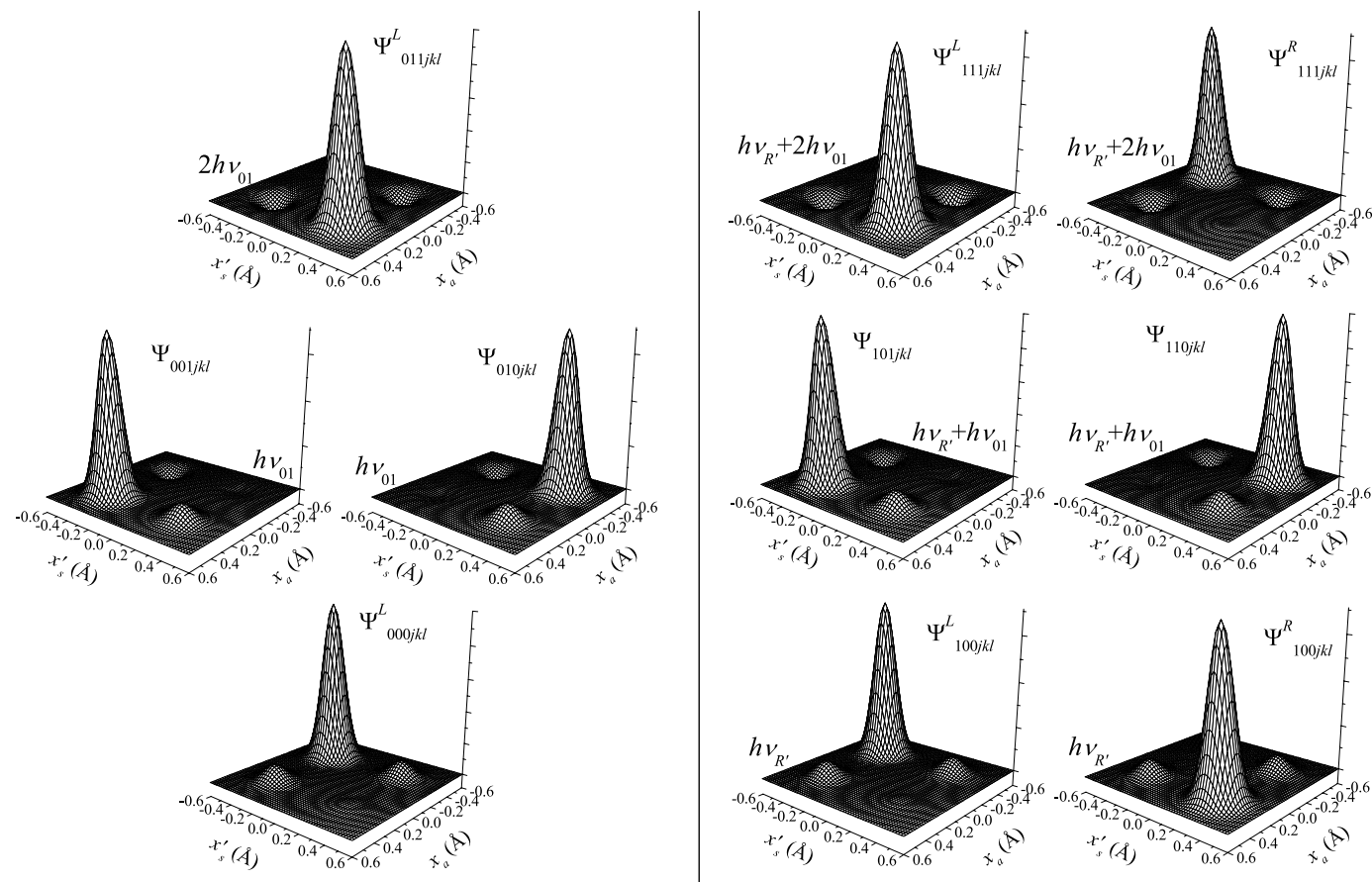


Fig. 6. Schematic view of the tunnelling wave functions for KHCO_3 (left hand side) and for benzoic acid (both sides). x_s and $x'_s = x_s \pm \sqrt{2}x_0$ are the normal coordinates for OH stretching modes. For the sake of clarity, the weak component of the wave function in one-dimension is multiplied by a factor of 2. The first index should be ignored for KHCO_3 .

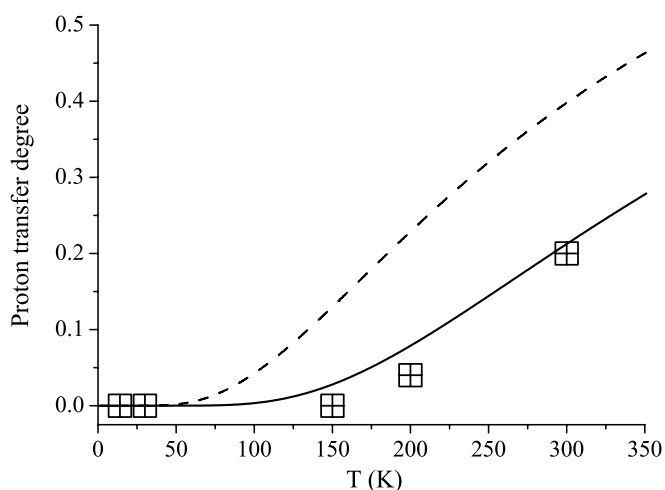


Fig. 7. Temperature effect on the proton transfer degree in the KHCO_3 crystal. \boxplus : experimental according to [22]. Solid line: Eq. (13) for two-levels. Dash line: Eq. (14) for three-levels.

sitory state undergoes fast re-entanglement to the upper state with probability $\exp(-2h\nu_{01}/kT)$. The fluctuation rate is then

$$\nu_b = 2\nu_{0b} \exp(-3h\nu_{01}/kT), \quad (15)$$

with $\nu_{0b} \approx 2.5 \times 10^{12} \text{ H s}^{-1}$, in proton per second units, and an Arrhenius slope of 648 cm^{-1} . This equation proves that an Arrhenius behaviour is not an unquestionable evidence for classical jumps.

QENS measurements were reported for a single-crystal of KHCO_3 , between 200 and 400 K, for momentum transfer parallel to the hydrogen bonds [16]. The inverse relaxation time (or attempt frequency), $\tau_0^{-1} = 2 \times 10^{12} \text{ s}^{-1}$ is sufficiently close to ν_{0b} to suggest that QENS and spectroscopy probe the same dynamics. On the other hand, the estimated activation energy $E_a = (336 \pm 32) \text{ cm}^{-1}$ is significantly different from $3h\nu_{01}$. A straightforward explanation for this apparent discrepancy is that the theoretical rate Eq. (15) and the measured one are different views of the same dynamics. The former accounts for coherent fluctuations of two pseudoprotons, with probability $\exp(-3h\nu_{01}/kT)$, and pre-factor $2\nu_{0b}$, while the latter, thanks to energy and momentum transfer, is an incoherent probe of a single partner, contributing to the coherent process with probability $\exp(-3h\nu_{01}/2kT)$, and pre-factor ν_{0b} . Hence, $3h\nu_{01}/2 = 324 \text{ cm}^{-1}$ accords with E_a . Because neutrons are plane waves, QENS is an incoherent probe of coherent oscillations of the proton probability rather than a probe of incoherent dynamics, amenable to stochastic jumps [16].

6.2. Benzoic acid

6.2.1. The rigid pair model

The interconversion rate of the benzoic acid crystal has been tentatively formalized by Skinner and Trommsdorff with uncorrelated stochastic jumps of proton pairs coupled

to the CO bonds [27]. Pairs were conceived of as rigid entities in an asymmetric double-well. It was supposed that (i) the potential asymmetry due to static effects of neighbouring dimers should be temperature dependent; (ii) coupling to phonons is necessary to mediate proton transfer at low temperatures; (iii) this coupling should quench coherent tunnelling and lead to incoherent phonon-assisted tunnelling; and (iv) a smooth transition to the Arrhenius behaviour of classical jumps should occur at elevated temperatures.

It should be emphasized that these hypotheses are not self-consistent. Pair dynamics cannot be simultaneously uncorrelated and coupled to phonons, which are coherent excitations of the crystal. Similarly, uncorrelated pair dynamics is irrelevant if the potential asymmetry is due to neighbouring molecules. In fact, this model ignores the spatial coherence intrinsic to crystals and describes a liquid-like surroundings. This leads to unrealistic low potential barriers and there is no evidence that the potential asymmetry could be actually temperature dependent [46]. Furthermore, the fluctuation rate at elevated temperatures deviates clearly from the Arrhenius behaviour [33].

6.2.2. Coherent phonon-assisted tunnelling

As for KHCO_3 , the potential functions in Table 2 are cornerstones for pseudoproton dynamics in benzoic acid. In addition, Raman spectra in the low-frequency range of crystals at various temperatures suggest some correlation between the proton transfer degree and the thermal population of a quasi-harmonic lattice mode at $h\nu_{R'} = (54 \pm 6) \text{ cm}^{-1}$ [37]. NMR and QENS suggest that the thermal population of this state could be a leading term for the interconversion rate at $T \leq 25 \text{ K}$ [33]. It is thus confirmed that interconversion is “phonon-assisted”, but the coupling is specific to a particular phonon that is not an acoustic mode and there is no evidence for decoherence. Consequently, dynamics should be rationalized with long-live macroscopic eigen states, and a tentative energy level scheme for pseudoprotons is presented in Fig. 6 [37].

- (i) Energy levels are labelled with quantum numbers, $n_{R'}$, n_a , n_s , for the lattice and pseudoproton states, respectively.
- (ii) In the ground state of the lattice mode ($n_{R'} = 0$), tunnelling levels and wave functions are similar to those for KHCO_3 (Fig. 6, left hand side).
- (iii) For $n_{R'} \geq 1$, the crystal switches to a superposition of L and R, leading to an equipartition of protons among sites (Fig. 6, right hand side). The potential surface for L is the same as in the $n_{R'} = 0$ state, while the potential asymmetry is reversed for R. The signs of the linear terms in $V(x_a)$ and $V(x_s)$ are changed, and so the lowest minimum of R corresponds to the highest minimum of L, and vice versa. The adiabatic separation is unaffected, which suggests that the lifetime of the phonon states is rather long, on the time scale of pseudoproton dynamics.

Table 2
Comparison of the spectroscopic and NMR-QENS [33] coefficients for the fluctuation rate Eq. (16), in proton per second and cm^{-1} units

	$v_{0b}\varepsilon^2$ (H s^{-1})	$h\nu_{R'}$ (cm^{-1})	$v_{0b}\varepsilon$ (H s^{-1})	$h(\nu_{01}-\nu_{R'})$ (cm^{-1})	v_{0b} (H s^{-1})	$h(2\nu_{01} + \nu_{R'})$ (cm^{-1})
Spectroscopy	2.0×10^8	54 ± 6	1.1×10^{10}	118 ± 6	7.2×10^{11}	398 ± 6
NMR-QENS	1.7×10^8	59	1.0×10^{10}	120	6.3×10^{11}	400

- (iv) The L and R tunnelling states, at $h\nu_{R'}$, $h\nu_{R'} + h\nu_{01}$, $h\nu_{R'} + 2h\nu_{01}$, are degenerate, and the wave functions are symmetrical with respect to $\{x_a = 0; x'_s = 0\}$. For the intermediate state at $h\nu_{R'} + h\nu_{01}$, L and R wave functions are identical.
- (v) Raman spectra (Fig. 5) do not evidence any significant coupling between νOH states for L and R. These states are therefore assumed to be separable. Then, according to the quantum theory of measurements [62], spectroscopy techniques probe one of the two configurations, with equal probabilities, and the spectra are unaffected by the superposition arising from thermal population of the lattice mode, as observed.

Compared to KHCO_3 , new interconversion processes arise from thermally induced transitions with $\Delta n_{R'} \neq 0$. In the sudden approximation, the probability depends on the overlap integral of the wave functions for the L and R states. In addition, wave-vector conservation for the phonon ($\mathbf{k}_{R'}$) and for protons (\mathbf{k}_H) imposes $\Delta \mathbf{k}_{R'} = \Delta \mathbf{k}_H = 0$, as for KHCO_3 . For $n_{R'} = 0$, $\mathbf{k}_{R'} = 0$ and $\mathbf{k}_{HL} = 0$ only for $n_a = n_s$. Alternatively, for $n_{R'} > 0$, there is no restriction for $\mathbf{k}_{R'}$, \mathbf{k}_{HL} or \mathbf{k}_{HR} , apart from $\mathbf{k}_{HL} + \mathbf{k}_{HR} = 0$ for $n_a = n_s$. Then, the leading terms of the fluctuation rate can be formulated as [37]:

$$v_b = v_{0b} \{ \varepsilon^2 \coth(h\nu_{R'}/2kT) + \varepsilon \exp[-(h\nu_{01} - h\nu_{R'})/kT] + \exp[-(2h\nu_{01} + h\nu_{R'})/kT] \}. \quad (16)$$

The first term represents the single-step interconversion $|000\rangle_L \leftrightarrow |100\rangle_R$, at $\mathbf{k}_{R'} = \mathbf{k}_H = 0$. $\coth(h\nu_{R'}/2kT)$, is the sum of up and down one-phonon transition rates, proportional to the Bose factor $n(\nu_{R'}) = [\exp(h\nu_{R'}/kT) - 1]^{-1}$ and to $[n(\nu_{R'}) + 1]$, respectively [27]; ε^2 is the overlap of the wave functions. (Note that $h\nu_{R'}$ was miss-interpreted by Skinner and Trommsdorff [27] as the potential asymmetry for the transfer of rigid pairs.)

The second term accounts for a single-step (single-pseudoproton) transfer $|100\rangle_R \leftrightarrow \{|010\rangle_L, |001\rangle_L\}$. Re-entanglement Eq. (12) is quenched by $\mathbf{k}_H \neq 0$. ε is the overlap factor. By contrast, transitions $|000\rangle_L \leftrightarrow \{|110\rangle_R, |101\rangle_R\}$ at $\mathbf{k}_H = 0$ do not contribute to the observed rate, because of fast re-entanglement.

The last term in Eq. (16) corresponds to the single-step interconversion: $|000\rangle_L \leftrightarrow |111\rangle_R$, at $\mathbf{k}_{R'} = \mathbf{k}_H = 0$. The overlap factor is unity. This transition is so far the best evidence for superposition of L and R in $n_{R'} \geq 1$ states. The $|100\rangle_R \leftrightarrow |011\rangle_L$ is not observed because the condition $\mathbf{k}_H = 0$ is realized only with a very low probability for the $|100\rangle$ state. Similarly, the two-stepwise mechanism

Eq. (15) observed for KHCO_3 is quenched by the very low probability for $\mathbf{k}_H = 0$ in the $\{|010\rangle, |001\rangle\}$ state.

Numerical values in Table 2 compare favourably with the best fit to measurements [33]. The pre-factor $v_{0b} \approx 1.8 \times 10^{11} \text{H s}^{-1}$ is the beating frequency. Compared to (15), the pre-factor 2 is cancelled because only $L \leftrightarrow R$ transitions with $\Delta n_{R'} \neq 0$ are relevant. Table 2 confirms that NMR and QENS probe macroscopically coherent quantum beats, rather than uncorrelated pairs [27]. It transpires that coupling between protons and phonons does not quench coherent tunnelling. In fact, the coupling gives rise to single-step processes much faster than the two-stepwise process for KHCO_3 .

In the crystal, the benzoic acid molecules pack in planar layers in which adjacent dimers are connected to each other by $\text{C}-\text{H} \cdots \text{O}$ contacts between oxygen atoms and hydrogens of the benzene ring [31]. The two contacts are slightly different at 20 K (2.519 and 2.474 \AA^{-1} , respectively) and basically equal to $\approx 2.55 \text{\AA}^{-1}$ at 175 K. It is tempting to speculate that unequal contacts in the $n_{R'} = 0$ state stabilize one of the crystal configuration, whereas equal contacts in the $n_{R'} \geq 1$ states lead to the superposition of L and R, degenerate in energy. This mechanism could be renamed as ‘‘phonon-assisted symmetry-breaking’’. Coupling terms should be more complex than the bilinear form introduced by Skinner and Trommsdorff [27].

7. Conclusion

In a defect-free crystal, atoms are not individual particles located at definite positions with definite momentums. They must be conceived of as macroscopic states in three dimensions, on the scale of the crystal size, and there is no possible transition to the classical regime of local behaviour.

For protons engaged in moderately strong hydrogen bonds, the adiabatic separation with respect to heavy atom dynamics unveils the macroscopic quantum behaviour of the sublattice of protons. For centrosymmetric dimers, normal coordinates lead to the non-commonsensual concept of macroscopic pseudoproton states and nonlocal potentials.

Interconversion proceeds through two coherent processes, clearly distinct. On the one hand, the proton transfer degree correlated with changes of the CO bond lengths characterizes the time-averaged extent of the chemical reaction. The crystal structure suggests a combination of macroscopic states with different dimer configurations in three-dimensions. On the other hand, quantum fluctuations of the probability density arise from interferences between

macroscopic tunnelling states. Energy-levels determined from spectroscopy provide the information necessary to calculate the proton transfer degree and the fluctuation rate at thermal equilibrium.

For KHCO_3 , the double minimum potential for pseudoprotons is perfectly isolated from lattice dynamics. Only the two-stepwise adiabatic interconversion is allowed. For benzoic acid, the potential asymmetry coupled to a particular phonon leads to three single-step sub-processes: two pairwise transfers and one single-pseudoproton transfer. The remarkable consistency of vibrational spectra with NMR and QENS data is a strong support to quantum interferences from cryogenic to room temperatures.

Despite substantial experimental progresses, more accurate neutron diffraction measurements of benzoic acid are needed. The superposition of L and R configurations and the dependence of the CO bond lengths with temperature should be re-examined. Evidences for macroscopic quantum entanglement should be sought after. Further studies of isotope mixtures are expected to emphasize the nonlocal nature of protons.

An intrinsic drawback of spectroscopy is the lack of information on the Born–Oppenheimer potential energy surface. It is thus difficult to make contact with quantum chemistry calculations. For benzoic acid, there is no information available so far on the nature of the coupling between protons and lattice modes. Although reasonably good potential barriers have been calculated [41,42,44], techniques bridging the gap between pseudoproton dynamics, purely quantum in nature, and the Born–Oppenheimer potential, are lacking.

References

- [1] P. Schuster, G. Zundel, C. Sandorfy, *The Hydrogen Bond. Recent Developments in Theory and Experiments. Vols. I, II and III*, North-Holland Publishing Co., Amsterdam, 1976.
- [2] P. Schuster, *Hydrogen Bonds*, Springer-Verlag, Berlin, 1984.
- [3] G.A. Jeffrey, W. Saenger, *Hydrogen Bonding in Biological Structures*, Springer-Verlag, Berlin, 1991.
- [4] C.L. Perrin, J.B. Nielson, *Annu. Rev. Phys. Chem.* 48 (1997) 511–544.
- [5] S. Scheiner, *Hydrogen Bonding: A Theoretical Perspective*, Oxford University Press, Oxford, 1997.
- [6] G. Lucazeau, A. Novak, *J. Raman Spectrosc.* 1 (1973) 573–586.
- [7] J.O. Thomas, R. Tellegren, I. Olovsson, *Acta Cryst. B* 30 (1974) 1155–1166.
- [8] J.O. Thomas, R. Tellegren, I. Olovsson, *Acta Cryst. B* 30 (1974) 2540–2549.
- [9] F. Fillaux, *Chem. Phys.* 74 (1983) 395–404.
- [10] F. Fillaux, *Chem. Phys.* 74 (1983) 405–412.
- [11] S. Benz, U. Haeblerlen, J. Tegenfeldt, *J. Magn. Res.* 66 (1986) 125–134.
- [12] S. Haussühl, *Solid State Commun.* 57 (8) (1986) 643–647.
- [13] F. Fillaux, J. Tomkinson, J. Penfold, *Chem. Phys.* 124 (3) (1988) 425–437.
- [14] S. Kashida, K. Yamamoto, *J. Solid State Chem.* 86 (2) (1990) 180–187.
- [15] M. Machida, Y. Yamaguchi, M. Sugimaya, Y. Iwata, N. Koyano, S. Fukui, *Physica B* 213–214 (1995) 393–395.
- [16] G. Eckold, H. Grimm, M. Stein-Arsic, *Physica B* 180–181 (1992) 336–338.
- [17] S. Kashida, S. Ikeda, Y. Nakai, *J. Phys. Soc. Jpn.* 63 (12) (1994) 4643–4647.
- [18] F. Fillaux, *Physica D* 113 (1998) 172.
- [19] S. Ikeda, F. Fillaux, *Phys. Rev. B* 59 (1999) 4134–4145.
- [20] F. Fillaux, A. Cousson, D. Keen, *Phys. Rev. B* 67 (2003) 054301, and 189901(E).
- [21] C. Odin, *J. Phys. Chem. B* 108 (2004) 7402–7411.
- [22] F. Fillaux, A. Cousson, M.J. Gutmann, *J. Phys.: Cond. Matter* 18 (2006) 3229–3249.
- [23] B.H. Meier, F. Graf, R.R. Ernst, *J. Chem. Phys.* 76 (2) (1982) 767–774.
- [24] S. Nagaoka, T. Terao, F. Imashiro, A. Saika, N. Hirota, S. Hayashi, *J. Chem. Phys.* 79 (10) (1983) 4694.
- [25] A. Gough, M.M.I. Haq, J.A.S. Smith, *Chem. Phys. Lett.* 117 (4) (1985) 363–389.
- [26] R. Meyer, R.R. Ernst, *J. Chem. Phys.* 86 (2) (1987) 784–801.
- [27] J.L. Skinner, H.P. Trommsdorff, *J. Chem. Phys.* 89 (2) (1988) 897–907.
- [28] A. Stöckli, B.H. Meier, R. Meyer, R.R. Ernst, *J. Chem. Phys.* 93 (3) (1990) 1502–1520.
- [29] A. Heuer, U. Haeblerlen, *J. Chem. Phys.* 95 (6) (1991) 4201–4214.
- [30] C.C. Wilson, N. Shankland, A.J. Florence, *Chem. Phys. Lett.* 253 (1996) 103–107.
- [31] C.C. Wilson, N. Shankland, A.J. Florence, *J. Chem. Soc., Faraday Trans.* 92 (1996) 5051–5057.
- [32] A.J. Horsewill, D.F. Brougham, R.I. Jenkinson, C.J. McGloin, H.P. Trommsdorff, M.R. Johnson, *Ber. Bunsenges. Phys. Chem.* 102 (3) (1998) 317–324.
- [33] M. Neumann, D.F. Brougham, C.J. McGloin, M.R. Johnson, A.J. Horsewill, H.P. Trommsdorff, *J. Chem. Phys.* 109 (17) (1998) 7300–7311.
- [34] S. Takeda, A. Tsuzuminati, *Magn. Reson. Chem.* 39 (2001) S44–S49.
- [35] M. Plazanet, N. Fukushima, M.R. Johnson, A.J. Horsewill, H.P. Trommsdorff, *J. Chem. Phys.* 115 (7) (2001) 3241–3248.
- [36] L. Latanowicz, E.C. Reynhardt, *Chem. Phys. Lett.* 341 (2001) 561–567.
- [37] F. Fillaux, M.-H. Limage, F. Romain, *Chem. Phys.* 276 (2002) 181–210.
- [38] M.R. Johnson, H.P. Trommsdorff, *Chem. Phys. Lett.* 364 (2002) 34–38.
- [39] Q. Xue, A.J. Horsewill, M.R. Johnson, H.P. Trommsdorff, *J. Chem. Phys.* 120 (23) (2004) 11107–11119.
- [40] L. Latanowicz, E.C. Reynhardt, J. Boguszyńska, *J. Mol. Struct. (Theochem)* 710 (2004) 111–117.
- [41] C.S. Tautermann, A.F. Voegelé, K.R. Liedl, *J. Chem. Phys.* 120 (2) (2004) 631–637.
- [42] Z. Smedarchina, A. Fernandez-Ramos, W. Siebrand, *J. Chem. Phys.* 122 (2005) 134309.
- [43] W. Wu, D.L. Noble, A.J. Horsewill, *Chem. Phys. Lett.* 402 (2005) 519–523.
- [44] F. Fillaux, F. Romain, M.-H. Limage, N. Leygue, *Phys. Chem. Chem. Phys.* 8 (2006) 4327–4336.
- [45] R.I. Jenkinson, A. Ikram, A.J. Horsewill, H.P. Trommsdorff, *Chem. Phys.* 294 (2003) 95–104.
- [46] L. Latanowicz, E.C. Reynhardt, *Chem. Phys. Lett.* 433 (2007) 444–449.
- [47] A.J. Horsewill, *Chem. Phys. Lett.* 433 (2007) 450–453.
- [48] V.M. Nield, D.A. Keen, Clarendon Press, Oxford, 2001.
- [49] A. Novak, *Struct. Bond. (Berlin)* 18 (1974) 177–216.
- [50] V.A. Benderskii, E.V. Vetoshkin, I.S. Irgibaeva, H.P. Trommsdorff, *Chem. Phys.* 262 (2000) 393–422.
- [51] V.A. Benderskii, E.V. Vetoshkin, H.P. Trommsdorff, *Chem. Phys.* 271 (2001) 165–182.
- [52] K. Giese, M. Petrović, H. Naundorf, O. Kühn, *Phys. Reports* 430 (2006) 211–276.
- [53] A. Witkowski, *J. Chem. Phys.* 47 (9) (1967) 3645–3648.
- [54] Y. Maréchal, A. Witkowski, *J. Chem. Phys.* 48 (8) (1968) 3697–3705.
- [55] S. Ikeda, S. Kashida, H. Sugimoto, Y. Yamada, S.M. Bennington, F. Fillaux, *Phys. Rev. B* 66 (2002) 184302.
- [56] O. Henri-Rousseau, P. Blaise, in: I. Prigogine, S.A. Rice (Eds.), *Adv. Chem. Phys.*, vol. 103, Wiley, New York, 1998, p. 1.

- [57] M. Boczar, K. Szczponek, M.J. Wójcik, C. Paluszkiwicz, *J. Mol. Struct.* 700 (2004) 39–48.
- [58] R.A. Cowley, *J. Phys.: Cond. Matter* 15 (2003) 4143–4152.
- [59] D.A. Keen, S.W. Lovesey, *J. Phys.: Cond. Matter* 15 (2003) 4937–4946.
- [60] H. Sugimoto, A. Okumura, H. Yuuki, *Phys. Rev. B* 73 (2006) 014305.
- [61] F. Fillaux, A. Cousson, *J. Phys.: Cond. Matter* 16 (2004) 1007–1010.
- [62] C. Cohen-Tannoudji, B. Diu, F. Laloë, Hermann, Paris, France, 1977.